

# Recent Development of Fabricating Flexible Micro-Supercapacitors for Wearable Devices

Chen Zhao, Yuqing Liu, Stephen Beirne, Joselito Razal, and Jun Chen\*

The rapid development in miniaturized personal wearable devices has significantly stimulated the pursuit for ultrathin, flexible, and lightweight energy storage devices. As one of the most promising power supply devices, supercapacitors have attracted great interest owing to their long operating lifetime, high power density, and fast charge–discharge rate. However, conventional supercapacitors pose challenges when being integrated with miniaturized wearable devices. In this regard, micro-supercapacitors with unique in-plane interdigitated electrode design provide flexibility and ease of integration with wearable and portable electronics. This review discusses the recent progress on fabrication strategies of interdigitated electrode arrays for flexible supercapacitors. Strategies toward their practical applications for powering integrated systems are presented. Finally, the future perspectives of flexible micro-supercapacitor are discussed.

## 1. Introduction

The rapid development of wearable integrated electronics, such as self-powered wireless sensor networks and personal physiological signal monitors, has greatly stimulated the demand for miniaturized flexible energy storage systems.<sup>[1–3]</sup> Currently, wearable electronics mainly rely on thin-film batteries or micro-batteries, which have been produced commercially to provide a system with required power and energy.<sup>[4]</sup> However, these batteries show some disadvantages and hinder their application in situations where extended use and high power are critical. Their first drawback is the limited operating lifetime; some devices usually require powering systems for several thousands of cycles. This issue is highlighted by the medical device sector

where a surgery is required to replace the batteries of an implanted device.<sup>[5]</sup> Another disadvantage is their low power density, which prevents their use in applications where high current is required (even over a short time).<sup>[6]</sup> Therefore, efforts to develop micro-energy storage devices with long operating lifetime and high power density provide complementary solutions to the shortcomings of batteries.

Supercapacitors (SCs) have been explored as a promising power supply device in recent years.<sup>[7]</sup> They are generally classified into two types based on their energy storage mechanisms:<sup>[8]</sup> 1) electrochemical double-layer capacitor (EDLC), which stores energy by the adsorption of anions and cations on the surface of


electrodes; and 2) pseudocapacitor which derives capacitance from the storage of charge in redox materials in response to a redox reaction. The active electrode materials for EDLCs are usually porous carbons, such as activated carbon,<sup>[9]</sup> carbon nanotubes,<sup>[10]</sup> graphene,<sup>[11,12]</sup> onion-like carbon,<sup>[13]</sup> and carbide-derived carbon.<sup>[14]</sup> There are also two main types of materials for pseudocapacitors: metal oxides (such as RuO<sub>2</sub> and MnO<sub>2</sub>)<sup>[15–17]</sup> and conducting polymers (such as polypyrrole, polyaniline, and polythiophene).<sup>[18–21]</sup> SCs can deliver superior energy in comparison to that of electrolytic capacitors, and possess a higher power density than that of batteries. The balanced energy density and power density that they provide bridge the gap between electrolytic capacitors and rechargeable batteries.<sup>[8]</sup> Furthermore, unlike batteries, SCs can last millions of cycles without losing their energy storage capacity.<sup>[22]</sup> These excellent properties make SCs promising energy storage devices which could replace or supplement batteries for miniaturized wearable electronics.

Conventional flexible SCs are fabricated using a vertical sandwich structure, containing two electrodes and solid-state electrolyte (Figure 1a).<sup>[23]</sup> This architecture attracted the most attention of researchers in the early development stage of this field due to its extremely simple structure and the relatively easy fabrication process of film electrodes. However, this design often suffers from ion transport limitations. Thick electrodes with increased mass loading of active materials are often required for high energy output. This increased thickness increases the ion transport resistance, leading to decreased power density.<sup>[24]</sup> Moreover, wearable electronics require flexible energy storage devices that have small volume,<sup>[25]</sup> which makes the conventional sandwiched architecture challenging to be integrated with miniaturized wearable devices. To overcome these problems,

Dr. C. Zhao  
School of Materials and Energy  
Guangdong University of Technology  
Guangzhou 510006, China

Y. Liu, Dr. S. Beirne, Prof. J. Chen  
Intelligent Polymer Research Institute and ARC Centre of Excellence  
for Electromaterials Science  
University of Wollongong  
Wollongong, NSW 2500, Australia  
E-mail: junc@uow.edu.au

Prof. J. Razal  
Institute for Frontier Materials  
Deakin University  
Geelong, VIC 3216, Australia

 The ORCID identification number(s) for the author(s) of this article can be found under <https://doi.org/10.1002/admt.201800028>.

DOI: 10.1002/admt.201800028

micro-supercapacitors (MSCs) with in-plane interdigitated microelectrodes have been developed (Figure 1b).<sup>[5,26]</sup>

The in-plane interdigitated design offers several merits over the stacked sandwich configuration. First, the interspace between electrode finger arrays can be precisely designed and controlled through advanced patterning technologies. By minimizing the distance between adjacent interdigitated electrodes, the ionic diffusion path between electrodes can be reduced and a small ion transport resistance can be achieved, resulting in an improved frequency response and increased power density.<sup>[13]</sup> Second, the electrode fingers are electrically isolated with neighboring ones, which greatly decreases the risk of device short circuit. Furthermore, as the edges of the interdigitated electrode fingers are also exposed to electrolyte, it can improve the diffusion of electrolyte ions and accessibility of the active electrode materials, leading to an enhanced rate performance (Figure 2).<sup>[27]</sup> This point is especially important for thick electrodes and electrodes made from 2D layered materials such as graphene, transition metal dichalcogenides (TMDs), and MXenes.<sup>[28–30]</sup> Finally, the in-plane interdigitated architecture could facilitate the integration with other small sized functional electronic devices on a planar substrate, which is beneficial to the miniaturization of the whole wearable system.<sup>[31,32]</sup> All of these advantages enable MSCs with in-plane interdigitated architectures to be the most promising candidate for energy storage components of miniaturized wearable electronics.

Wearable systems are generally designed to be thin, lightweight, and flexible. Such properties are also required for the MSCs to be integrated. Soft plastics, such as polyethylene terephthalate (PET),<sup>[11,33]</sup> Scotch tape,<sup>[34]</sup> polydimethylsiloxane (PDMS),<sup>[35]</sup> paper,<sup>[36,37]</sup> and even textile<sup>[38]</sup> are employed as substrates for flexible MSCs (fMSCs). Active electrode materials and solid-state electrolytes used for fabrication of flexible solid-state sandwiched SCs can be utilized for fMSCs as well; more details about these materials can be found in other review papers.<sup>[23,39]</sup> However, until now, there has not been a universal fabrication method that is compatible with all active materials as different materials possess different properties. There are already some reviews on the development of MSCs.<sup>[22,40–42]</sup> However, they either failed to discuss the fabrication strategies of fMSCs<sup>[41]</sup> or failed to introduce the applications of fMSCs in integrated systems.<sup>[22,40]</sup> In this mini review, we will discuss how different active materials can be used for fabrication of fMSCs through different fabrication strategies. We will also introduce some of the latest achievements in integrated systems based on fMSCs. Finally, we will provide insights into the future development trends for the fMSCs.

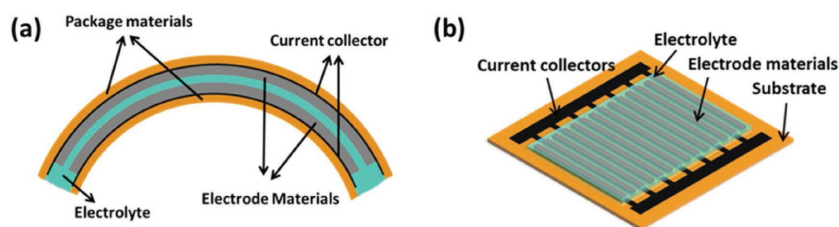
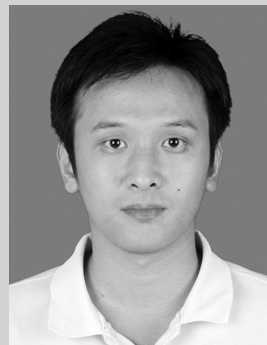


**Figure 1.** Schematic illustration of flexible supercapacitors with a) conventional sandwiched structure, and b) interdigitated structure.



**Chen Zhao** is currently an associate professor at the School of Materials and Energy, Guangdong University of Technology. He received his B.S. and M.S. degrees from the Huazhong University of Science and Technology, China, and his Ph.D. degree from the University of Wollongong, Australia. His current research interests focus on materials and device engineering of flexible and stretchable energy storage devices and sensors for wearable electronics.



**Yuqing Liu** received her BS degree from the School of Materials Science and Engineering, Zhengzhou University, China in 2013. She is a current PhD student at the Intelligent Polymer Research Institute, University of Wollongong, Australia under the supervision of Prof. Jun Chen. Her current research

is focused on the fabrication and design of wearable energy devices.



**Jun Chen** is currently appointed as a Full Professor at the IPRI, Australian Institute of Innovative Materials, University of Wollongong, Australia. He completed his PhD degree at the School of Chemistry, UOW, Australia, in 2003. Prof. Chen is a Chief Investigator of The ARC Centre of Excellence for Electromaterials Science

(ACES) with extensive skills in electroactive materials and sustainable chips/devices, and demonstrated experience in High-Tech spin-off companies. His current research interests include: soft chip systems, electro-/biointerfaces/inks, nano-/micromaterials, and printable device design and fabrication.

## 2. Fabrication Strategies for Interdigitated Microelectrode Arrays

Contrary to the relatively easy fabrication of flexible sandwiched SCs, the fabrication of fMSCs with interdigitated design involves additional patterning steps before or after the formation of flexible film electrode. This step is crucial as the properties of the electrode

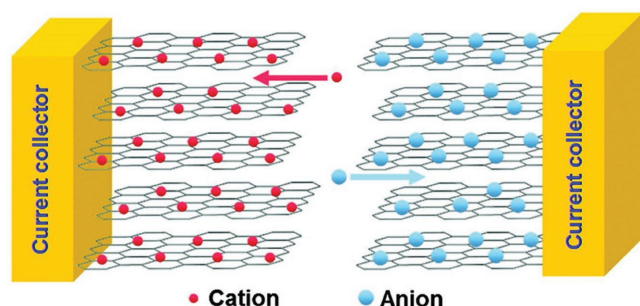


**Figure 2.** Schematic illustration of the operating principle of MSCs with graphene electrodes. Reproduced with permission.<sup>[27]</sup> Copyright 2011, American Chemical Society.

fingers determine the electrochemical performance of fabricated MSCs. At present, most MSCs are produced at laboratory scale and no commercial MSCs are available for practical industry level applications. However, the rapid development of micromanufacturing has enabled various microfabrication techniques to be applied for the patterning of electrode fingers. These fabrication methods can be mainly classified into four categories: 1) deposition of active materials on prepatterned current collectors; 2) laser writing of active materials; 3) etching–patterning of active material films; and 4) direct printing of active materials.

### 2.1. Deposition of Active Materials on Prepatterned Current Collectors

In this method, interdigitated current collectors are fabricated on flexible substrates either by photolithography or by direct metal deposition through a mask, followed by the deposition of active materials. Various methods such as electrochemical polymerization, electrolytic, electrophoretic, and chemical deposition can be used for the deposition of active materials.<sup>[22]</sup>

Photolithography is a process used in microfabrication to obtain patterns on a substrate. It is widely used in micro-electromechanical system (MEMS) and microchip production due to its high resolution. Photoresists with complex patterns can be created through corresponding photomasks. A general approach is to prepare current collector arrays via photolithography and a wet-etching process. Active materials are then subsequently deposited. The first MSCs with interdigitated electrode arrays were reported by Lee and co-workers in 2003.<sup>[20]</sup> In their report, gold or platinum microelectrode arrays were produced on a silicon substrate by the photolithography and wet-etching method. Conducting polymers, such as polypyrrole (PPy) and poly-(3-phenylthiophene) were electrochemically polymerized onto these microelectrode arrays to form polymer-interdigitated MSCs with 50 parallel-connected pairs of microelectrodes. The width of the microelectrodes and the distance between them were designed to be both 50  $\mu\text{m}$ . By choosing 0.1 M aqueous  $\text{H}_3\text{PO}_4$  solution and 0.5 M  $\text{Et}_4\text{NBF}_4/\text{acetonitrile}$  as electrolytes, a cell voltage between 0.6 and 1.4 V and cell capacitance ranging from 1.6 to 14 mF were obtained. However, practical applications for wearable electronics require flexible and leakage-free devices. As such, solid-state or gel electrolytes are preferred. MSCs have been further improved using a polymer gel electrolyte (Figure 3).<sup>[43]</sup> The same

fabrication process was carried out to produce PPy-coated gold microelectrode arrays on a silicon substrate. A layer of solidified poly(vinyl alcohol) (PVA)/ $\text{H}_3\text{PO}_4$  gel electrolyte film was then firmly attached to the PPy microelectrode arrays. The PPy microelectrodes could be detached from the silicon substrate and attached onto the gel electrolyte film to form a flexible, solid-state MSC because the adhesion between the PPy microelectrodes and gel electrolyte film was stronger than that between PPy and gold. The gel electrolyte film served not only as an electrolyte but also a structural substrate for the whole device. Furthermore, the device can be rolled up and folded without deterioration of the electrochemical properties. This device demonstrated the feasibility of fabricating flexible solid-state MSCs from a combined photolithography and electrochemical deposition method.

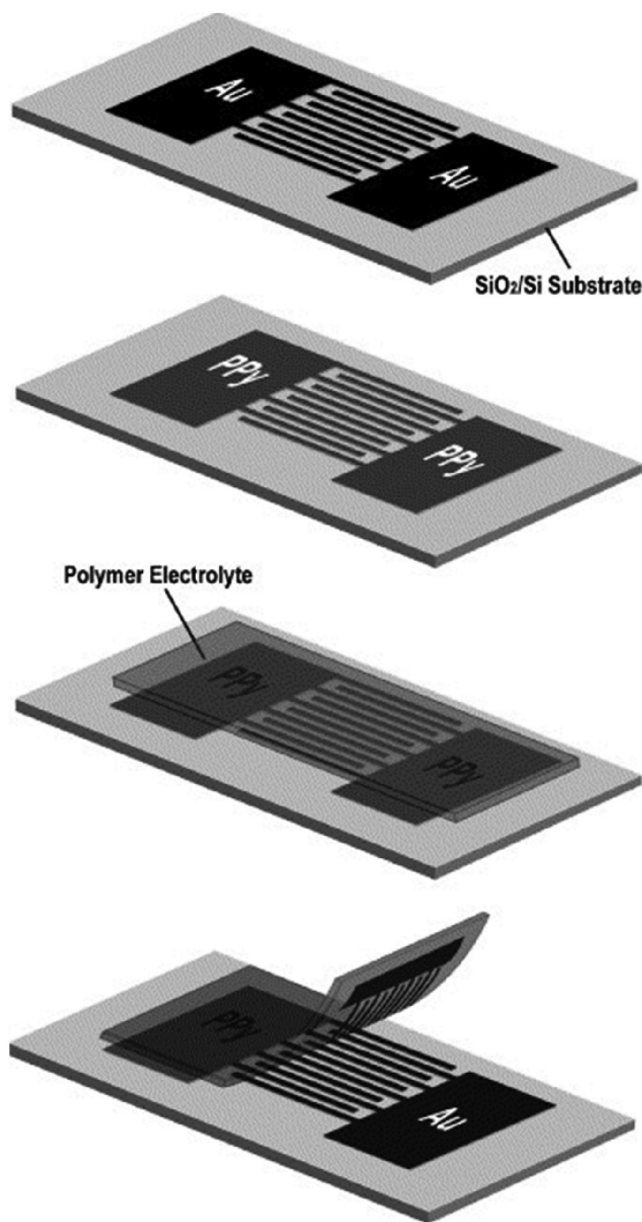


**Figure 3.** Schematic diagrams of the procedure for fabricating flexible solid-state MSCs. Reproduced with permission.<sup>[43]</sup> Copyright 2006, Elsevier Ltd.



After the pioneering work of PPy-based flexible solid-state MSCs, significant efforts have been devoted to fabricate fMSCs using nanostructured carbon materials, such as carbon nanotubes (CNTs), graphene, and their composites. Ha and co-workers fabricated a fMSC with functionalized multiwalled carbon nanotubes (MWNTs) with poly(ethylene glycol) diacrylate (PEGDA)-based ion gel (Figure 4a,b).<sup>[44]</sup> After the deposition of interdigitated Ti/Au current collectors on a PET substrate through photolithography, a functionalized MWNT solution in deionized (DI) water was spray-coated onto the current collectors. The ion gel, which was prepared by mixing PEGDA with ionic liquid 1-ethyl-3-methylimidazolium bis(trifluoromethylsulfonyl)imide ([EMIM][TFSI]), was drop-cast on to the fMSC. The fMSC had interdigitated electrodes with an interspace of 150  $\mu\text{m}$  and a width of 500  $\mu\text{m}$ . With a 500 nm thick MWNT layer, the fMSC could deliver a capacitance of 5.3 F  $\text{cm}^{-2}$  at a scan rate of 0.01 V  $\text{s}^{-1}$  with a wide voltage window of 2 V. This device also showed good mechanical stability with only 5% loss in capacitance after 1000 bending cycles to a bending diameter of 3 mm. Graphene is also a robust and attractive material for fMSCs. Niu et al. fabricated a flexible, ultrathin, and solid-state MSC based on ultrathin reduced graphene oxide (rGO) and PVA/ $\text{H}_3\text{PO}_4$  gel electrolyte.<sup>[11]</sup> The interdigitated Au current collector arrays were fabricated on PET by metal thermal evaporation and photolithography. Subsequently, graphene oxide (GO) sheets were deposited on the Au patterns through electrophoretic deposition. GO sheets were chemically reduced by hydrazine monohydrate to obtain conductive rGO-interdigitated microelectrodes (400  $\mu\text{m}$  width, 400  $\mu\text{m}$  spacing, and 25 nm thickness). Finally, PVA/ $\text{H}_3\text{PO}_4$  was cast on the interdigitated microelectrodes. The shortened diffusion path lengths and the open edges of the rGO microelectrodes enhanced the diffusion of electrolyte into the layers of rGO, resulting in improved total accessible electrochemical surface area. Consequently,

the solid-state MSCs achieved a high areal capacitance of 472  $\mu\text{F cm}^{-2}$  and volume capacitance of 359 F  $\text{cm}^{-3}$ .

In addition to photolithography, metal deposition through a designed mask is also explored to fabricate interdigitated current collector arrays. The mask can be produced by laser cutting, laser printing, and pen drawing. For example, Wang and co-workers reported a flexible textile-based MSC by laser-scribing masking (Figure 4c,d).<sup>[38]</sup> A fabric cloth was sealed with Kapton tape on both sides. A laser with controlled intensity was applied to cut through the top Kapton layer without causing damage to the sealed fabric. Electroless deposition of Ni and hydrothermal reduction of GO lead to the rGO-coated Ni microelectrodes (1.5 mm width and 0.5 mm spacing) on the exposed textile. The solid-state textile MSC with PVA/ $\text{H}_3\text{PO}_4$  gel electrolyte showed an areal capacitance of 8.19 mF  $\text{cm}^{-2}$  at a scan rate of 0.01 V  $\text{s}^{-1}$ . It could be bent to 180° without noticeable capacity degradation. Ye and co-workers utilized a printed sacrificial mask to prepare flexible solid-state MSCs based on interdigitated Au/polyaniline (PANi) network hybrid electrode.<sup>[45]</sup> In a typical process, an interdigitated circuit template is printed on PET by a laser printer. Then, Au with a thickness of 80 nm was deposited on the printed PET via electron beam evaporation. Interdigitated Au electrodes were obtained by removal of the printed circuit template. PANi nanowire networks were in situ electropolymerized on the Au current collector arrays. PVA/ $\text{H}_2\text{SO}_4$  gel solution was drop-cast onto the surface of the Au/PANi hybrid microelectrodes. The flexible solid-state MSC was achieved after the electrolyte gel was solidified. With 300 s deposition of PANi, the flexible solid-state MSC (electrode arrays with 300  $\mu\text{m}$  width and 300  $\mu\text{m}$  spacing) delivered an areal capacitance of 26.49 mF  $\text{cm}^{-2}$  at a current density of 0.1 mA  $\text{cm}^{-2}$ . It also showed excellent flexibility with nearly unchanged electrochemical performance when bent to 90°. Similar to the laser-printed template approach, Alshareef and co-workers used marker pen to draw the sacrificial mask to produce interdigitated microelectrodes.<sup>[46]</sup>

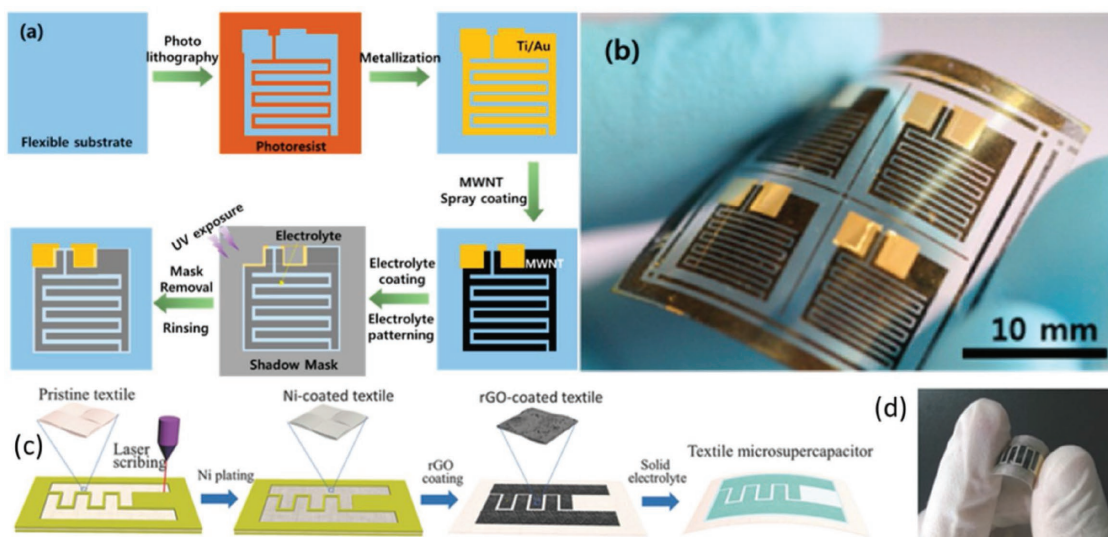


**Figure 4.** a) Schematic diagrams of the procedure for fabricating fMSC with functionalized multiwalled carbon nanotubes and patterned solid-state electrolyte on a PET substrate. b) Photographic image of fabricated fMSCs. c) The scheme of the fabrication process of textile MSCs. d) The photo of a solid-state textile MSC. a–b) Reproduced with permission.<sup>[44]</sup> Copyright 2015, American Chemical Society. c–d) Reproduced with permission.<sup>[38]</sup> Copyright 2016, Wiley-VCH.

The sacrificial ink patterns were drawn on substrates using commercial marker pens. After metal and conducting polymer deposition, the ink pattern was removed by organic solvents to achieve the interdigitated electrode arrays. The width and interspace between the electrode fingers were about 500 and 450  $\mu\text{m}$ , respectively. A fMSC fabricated on polyethylenephthalate substrate employing poly(3,4-ethylenedioxythiophene) (PEDOT) as active materials showed a maximum energy density of 9  $\text{mWh cm}^{-3}$ . And, it exhibited stable electrochemical performance at bending state.

Deposition of active materials on prepatterned current collectors is also suitable for fabricating fMSCs with asymmetric electrode arrays which contain both carbon and pseudocapacitive materials. The pseudocapacitive electrodes can serve as the energy source, while the carbon electrodes provide a high power supply. Furthermore, asymmetric devices often possess a wider operating voltage window than symmetric systems (usually less than 1.0 V), leading to a higher energy density. A flexible asymmetric MSC with  $\text{Co(OH)}_2$  and electrochemically reduced graphene oxide (erGO) was demonstrated by Jun and co-workers. An operating voltage of 1.4 V and an energy density of 0.35  $\mu\text{Wh cm}^{-2}$  were achieved.<sup>[47]</sup>

In this category, various materials such as nanostructured carbons, metal oxides, and conducting polymers can be used to produce interdigitated microelectrodes for MSCs. This provides abundant opportunities for choosing appropriate active materials to meet the requirements of practical applications (high energy or high power). Photolithography possesses advantage in high resolution electrode array fabrication. A narrow interspacing of 50  $\mu\text{m}$  can be achieved, which is promising for high power applications. However, patterning with photoresists and etching are cumbersome for widespread application. Making patterns through masks is simple and cost-effective. This approach opens up new avenues for easy and scalable fabrication of fMSCs despite of its relatively low resolution ( $\approx 300 \mu\text{m}$  for laser-printed mask,  $\approx 500 \mu\text{m}$  for marker pen).

Thus, researchers are still on the way to seek for simple, low-cost, and high-throughput techniques to fabricate fMSCs with high performance.

## 2.2. Laser Writing of Active Materials

Laser scribing is a cost-effective method to fabricate interdigitated microelectrode without additional masks and complex processing. It has shown great potential for large-scale production and commercialization of fMSCs. GO can be reduced to highly conductive rGO upon laser irradiation because of the photothermal effect.<sup>[48]</sup> Thus, it is possible to generate conductive rGO patterns with micrometer resolution on GO films through laser reduction. Based on the laser reduction method, Ajayan and co-workers created in-plane MSCs on a single piece of hydrated GO paper.<sup>[49]</sup> The unreduced hydrated GO between the laser-reduced rGO-interdigitated electrodes acted as both the electrolyte and separator owing to its high ionic conductivity and electric insulation. The reported in-plane MSC with a circular geometry could deliver an areal capacitance of 0.51  $\text{mF cm}^{-2}$ . The thickness of the rGO patterns can be easily regulated by changing the laser power. Although this method is promising, the large internal resistance (6.5  $\text{k}\Omega$ ) of the device is not sufficient for practical application. Later, El-Kady and Kaner developed a scalable fabrication method for rGO-based MSCs on GO film using a standard LightScribe digital video disc (DVD) burner.<sup>[50]</sup> A DVD disk was coated with a film of GO and with the laser from the DVD burner, interdigitated patterns designed on the computer were transferred onto the GO film to get the desired rGO patterns. By this method, more than 100 MSCs could be readily generated on a single disk in 30 min (Figure 5). With a layer of PVA/ $\text{H}_2\text{SO}_4$  gel electrolyte, the fabricated MSC exhibited an areal capacitance of 2.32  $\text{mF cm}^{-2}$ . The device also showed an excellent flexibility with 97% retention of the initial capacitance after 2000 bending cycles. With an ionic

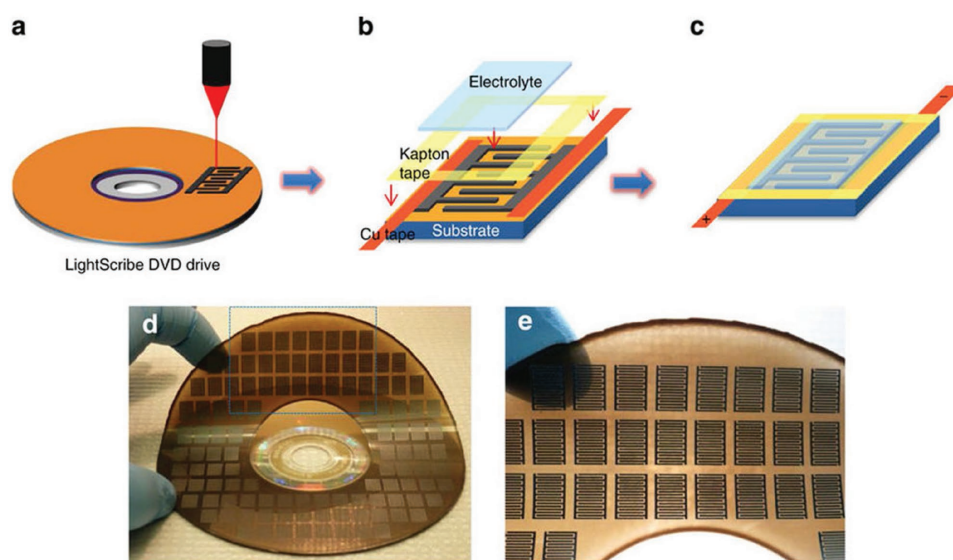


**Figure 5.** a–c) Schematic illustration of the fabrication process for laser-scribed graphene-based fMSCs. d,e) More than 100 fMSCs on a GO film. Reproduced with permission.<sup>[50]</sup> Copyright 2013, Nature Publishing Group.

liquid-based ionogel as the electrolyte, the operating voltage could be enlarged to 2.5 V. Later, the same group created hybrid electrode-based MSCs using the laser-scribing technique. By using the laser to irradiate the GO/RuCl<sub>3</sub> composite film, the Ru<sup>3+</sup> (RuCl<sub>3</sub>) in the composite film was simultaneously oxidized to hydrous RuO<sub>2</sub> with the reduction of GO to rGO in order to form rGO/RuO<sub>2</sub> hybrid microelectrodes.<sup>[51]</sup>

According to Tour and co-workers' report, sp<sup>3</sup>-carbon atoms of commercial polymer films such as polyimide (PI) can be thermally converted to sp<sup>2</sup>-carbon atoms in ambient conditions by pulsed CO<sub>2</sub> infrared laser irradiation.<sup>[52]</sup> Porous graphene films with 3D networks can be formed on the surface of PI. The interdigitated graphene microelectrodes with high conductivity can serve as both the active electrodes and the current collectors. The fMSC showed an areal capacitance greater than 9 mF cm<sup>-2</sup> at a current density of 0.02 mA cm<sup>-2</sup> using PVA/H<sub>2</sub>SO<sub>4</sub> gel electrolyte.<sup>[53]</sup> The same group went on to fabricate high-performance MSCs from boron-doped porous graphene, which were created by the same laser writing process on boric acid-containing PI sheets. As a result of boron doping, the as-prepared fMSCs achieved an areal capacitance of 16.5 mF cm<sup>-2</sup> at a current density of 0.05 mA cm<sup>-2</sup>.<sup>[54]</sup> Asymmetric fMSCs can also be produced by combining electrodeposition of materials with different potential windows onto two arrays of microelectrodes.<sup>[55]</sup> Watanabe and co-workers demonstrated a fMSC on PI films using a compact semiconductor blue-violet laser with a 405 nm beam that can be almost totally absorbed in the PI film.<sup>[56]</sup> The fMSC with PVA/H<sub>2</sub>SO<sub>4</sub> gel electrolyte exhibited an areal capacitance of 28 mF cm<sup>-2</sup> at a current density of 0.05 mA cm<sup>-2</sup>. After plasma treatment, the hydrophobic surface of the graphene obtained by laser writing became superhydrophilic, leading to an improved performance with a 13.9% enhancement (≈32 mF cm<sup>-2</sup>) at the same current density of 0.05 mA cm<sup>-2</sup>.<sup>[57]</sup>

The direct laser writing of interdigitated microelectrodes is a simple, powerful, low-cost, and high-throughput technique to fabricate fMSCs. It does not require additional masks, or complicated processing operations, making it promising for large-scale production of fMSCs. However, this technique is currently limited to graphene-based MSCs and is not applicable to a wider variety of active materials.

### 2.3. Etch Patterning of Active Film

Over the past decade, flexible and robust film electrodes with advanced nanostructures and superior performance have been developed from a wide range of electrode materials (including carbon materials,<sup>[58,59]</sup> conducting polymers,<sup>[60]</sup> metal oxides,<sup>[61]</sup> and binary<sup>[62]</sup> or ternary composite materials<sup>[63,64]</sup>) via various technologies (e.g., spray coating,<sup>[65]</sup> vacuum filtration,<sup>[63]</sup> electrospinning,<sup>[60]</sup> and electrophoretic deposition<sup>[66]</sup>). Generating interdigitated electrodes directly from these well-developed films is an effective strategy to maintain the nanostructures of these materials and pursue high-performance fMSCs. In this approach, interdigitated electrodes are achieved by etching the unwanted materials away from the film and directly assembling into solid-state fMSCs after a gel electrolyte coating. Etching techniques including dry etching (i.e., plasma<sup>[67]</sup> or laser<sup>[68]</sup>) and wet etching (microfluidic etching<sup>[69]</sup>) have been employed

and a prepatterned mask, template, or software program was used for the design of electrode patterns.

#### 2.3.1. Plasma Etching

Plasma etching is the mostly used dry-etching technique to fabricate interdigitated electrodes from films. This method etches various electrode materials by shooting at the exposed sample a high-speed stream of glow discharge (plasma) of appropriate gas mixture.<sup>[70–72]</sup> Specifically, a thin layer of current collector material (e.g., Au) with interdigitated patterns is sputter or evaporatively coated onto film electrode through a customized mask or by photolithography. Films with the patterned current collector coatings are irradiated in a plasma chamber and the exposed part of electrode materials etched to form interdigitated electrodes. The irradiation duration varies according to the film thickness and repeated etching is necessary for films with thickness greater than 1 μm.<sup>[72]</sup>

As an example, Wu et al. fabricated a graphene-based fMSC with ultrahigh power density by plasma etching a graphene thin film on PET substrate.<sup>[72]</sup> In this work, a novel reduction method using methane plasma was introduced to treat the spin-coated GO film to provide additional carbon sources (i.e., C<sup>+</sup>, CH<sub>n</sub><sup>+</sup>, and CH<sub>n</sub>, *n* = 1–3), which gave rise to high C/O ratio (9.2:1) and high electrical conductivity (345 S cm<sup>-1</sup>) for the reduced graphene film. The fMSCs derived from methane plasma graphene (MPG) film exhibited superior capacitance (80.7 μF cm<sup>-2</sup> and 17.9 F cm<sup>-3</sup>, based on the area and volume of the whole device, respectively) and showed ultrahigh power density of 495 W cm<sup>-3</sup>. Another fMSC made from plasma-etched alternating stacked graphene-conducting polymer compact film (**Figure 6**) was also reported by this group.<sup>[67]</sup> The 2D pseudocapacitive polyaniline-functionalized graphene nanosheets (PANi-G) and electrochemically exfoliated graphene (EG) were alternately deposited via vacuum filtration and transferred to a flexible substrate (i.e., PET). The highly conductive EG offers electron-conducting pathway for good rate capability of the fMSC, while also providing an elastic spatial confinement effect to buffer the large volume change of redox PANi-G sheets during the charge–discharge process for stable cycle life (92.6% at 1000 cycles). The fMSC device with the plasma-etched interdigitated electrodes exhibited extremely high device areal capacitance of ≈52.5 mF cm<sup>-2</sup> and volumetric capacitance of ≈109 F cm<sup>-3</sup> due to the presence of mesoporous and pseudocapacitive PANi-G sheets with easily accessible ion-transporting channels.

In addition to fMSCs based on carbons and polymers, plasma etching is also applicable for fMSCs made from films containing metal oxides. Tay and co-workers reported a fMSC fabricated from a vacuum filtrated rGO/manganese dioxide (MnO<sub>2</sub>)/silver nanowire (AgNW) ternary hybrid thin film (RGMA ternary hybrid film).<sup>[70]</sup> The device displayed exceptionally high rate capability (up to 50 V s<sup>-1</sup>) due to the enhanced electrical conductivity introduced by the conducting AgNW bridges between the graphene sheets or needle-like MnO<sub>2</sub>. An electrospun porous NiFe<sub>2</sub>O<sub>4</sub> nanofiber film was also plasma-etched to form fMSC with the use of photolithographically prepatterned Ni current collector as mask.<sup>[71]</sup> A specific capacitance of 2.23 F cm<sup>-3</sup>, excellent rate capability, and robust cycling stability (93.6%



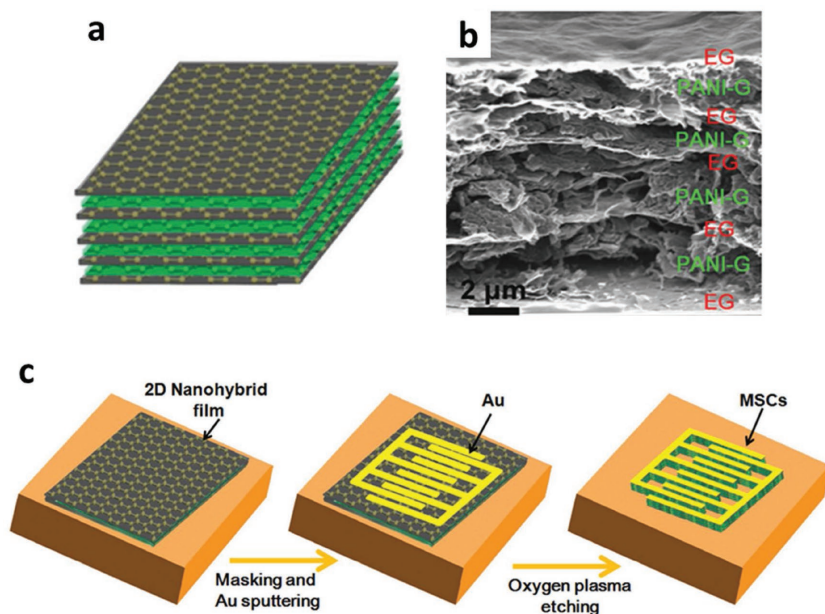


**Figure 6.** a) Schematic of micrometer-thick 2D nanohybrid film, showing layer-stacked structure. b) Scanning electron microscope (SEM) image of 2D nanohybrid film. c) Illustration of the fabrication procedure for in-plane fMSCs with interdigital fingers. All panels reproduced with permission.<sup>[67]</sup> Copyright 2015, Wiley-VCH.

capacitance retention after 10 000 cycles) were achieved. This work shows the feasibility of plasma etching on a wide range of materials and the effectiveness in maintaining the superior nanostructures and performance of electrode films. However, most of the plasma-etching processes rely on masks for the development of the designed patterns, which are labor-intensive and sensitive to patterning parameters. To solve this problem, a novel mask-free plasma-scanning method was developed by Wu and co-workers.<sup>[73]</sup> As shown in **Figure 7**, an atmospheric pulsed microplasma jet was generated at the end of a XYZ-motored nozzle and etched a CNT film along the path drawn in the software of a computer. A minimum width of 60 μm of the etched lines can be achieved when etching parameters (i.e., voltage, pulse frequency, pulse width, content of O<sub>2</sub> in mixed gases, scanning speed, and height of the nozzle) were carefully controlled. Compared with the mask-involved plasma etching, this technique enables freedom adjustment in pattern parameters, does not require masks and postprocessing, and is a more scalable and effective technology.

### 2.3.2. Laser Etching

In recent years, the laser lithography technology (known as laser cutting) is used gradually as an etching tool to create patterned channels on film electrodes. Similar with the microplasma jet technique, laser etching system uses a XY-controlled laser spot to etch materials quickly along a route as designed in computer software. Films consisting of various electrode materials like activated mesophase pitch (aMP),<sup>[68]</sup>

mushroom-derived carbon (MDC),<sup>[74]</sup> rGO–PEDOT/poly(styrenesulfonate) (PSS),<sup>[75]</sup> and Mxene<sup>[34]</sup> have been laser-etched into interdigitated form for use as fMSC device. For instance, Liu et al. fabricated a fMSC from a rGO–PEDOT/PSS film with high film thickness of 58 μm and a minimum width of etched lines of 100 μm (**Figure 8a,c**).<sup>[76]</sup> The device achieved a high areal capacitance of ≈84.7 mF cm<sup>-2</sup> and a volumetric capacitance of ≈14.5 F cm<sup>-3</sup>. The simplicity and convenience design of varying patterns was demonstrated by laser etching 10 fMSCs with different microelectrode widths in 90 s (**Figure 8b**). In addition, they also demonstrated the potential in practical application by lighting 20 light-emitting diode (LED) lights using 12 connected fMSCs in 6 series and 2 parallel, in which the connections were also simply established by laser etching. It is believed that this technology can be applied to a wide range of electrode materials and film thicknesses provided that residual precursors (or any unwanted materials) can be completely removed to create well-separated microelectrodes. The simplicity of this technology (i.e., computer-generated intricate patterns that can be “written” on materials such as polymers, nanomaterials, and many others on desired substrates with complex shapes and structures) can pave the way for the rational engineering of novel materials that are suitable for a wide range of wearable electronic devices.

### 2.3.3. Microfluidic Etching

Microfluidic etching, a wet-etching technique, was also used to create patterned channels on electrode films. For example, Xue et al. prepared a MnO<sub>2</sub>-based fMSC by microfluidic etching the electrospun MnO<sub>2</sub> films.<sup>[69]</sup> In this work, a thin layer of MnO<sub>2</sub> nanofiber film was first prepared via electrospinning, which was transferred onto solid polymer gel electrolyte film and then coated with a layer of indium tin oxide

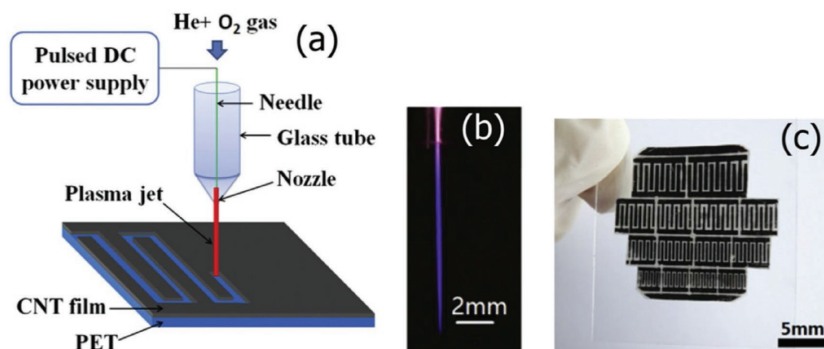


**Figure 7.** a) Schematic diagram of the experimental setup. b) Photographic image of the microplasma jet. c) Interdigitated CNT electrodes with different sizes on PET substrate. All panels reproduced with permission.<sup>[73]</sup> Copyright 2017, Elsevier Ltd.

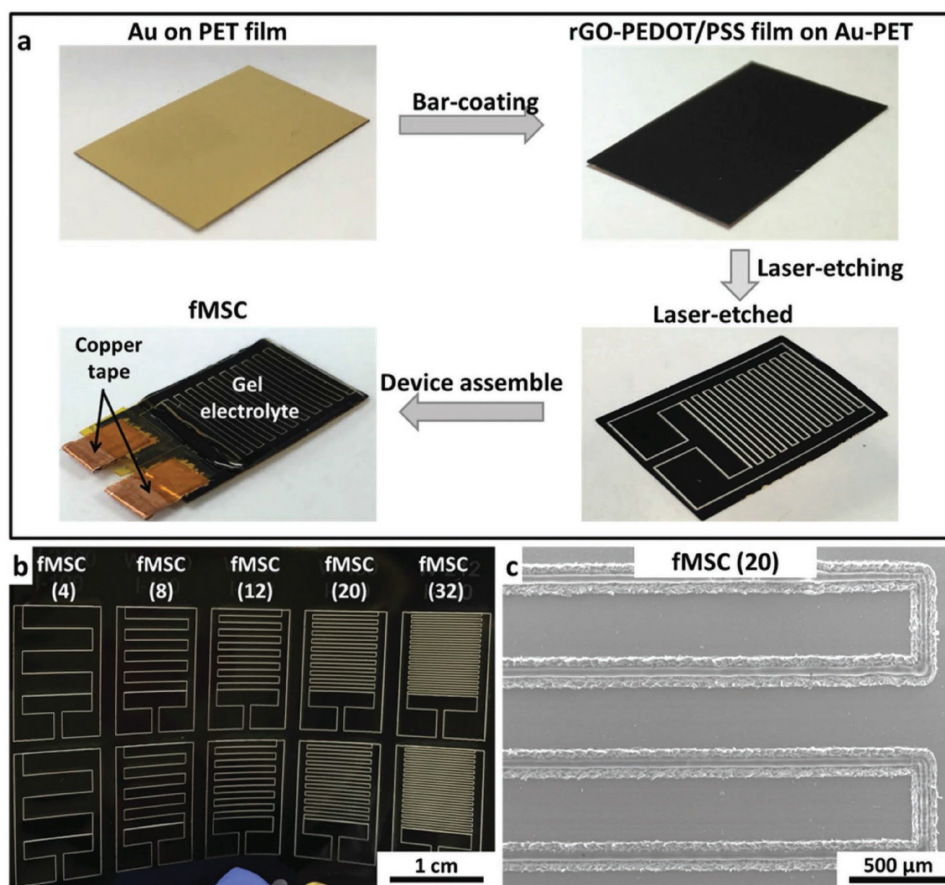


**Figure 8.** a) Schematic diagram of the fabrication of all-solid-state rGO-PEDOT/PSS-based planar fMSCs on a flexible PET film using laser cutter technique. b) Photo images of laser-etched fMSCs with different configurations on one rGO-PEDOT/PSS film. c) SEM image of fMSC (20) pattern (top view). All panels reproduced with permission.<sup>[75]</sup> Copyright 2016, Wiley-VCH.

(ITO) (Figure 9 steps (a, b). Afterward, microfluidic etching was used to prepare MnO<sub>2</sub>/ITO-interdigitated microelectrodes, as shown in Figure 9 step (c). Specifically, a PDMS stamp with

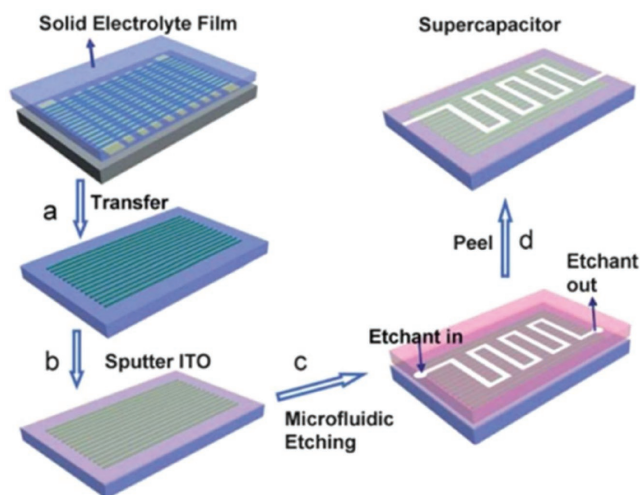


**Figure 9.** Schematic diagram – the fabrication of micro-supercapacitors via the microfluidic etching. Reproduced with permission.<sup>[69]</sup> Copyright 2011, Royal Society of Chemistry.

interdigitated patterns was pressed onto the MnO<sub>2</sub>/ITO film, forming microfluidic channels between the MnO<sub>2</sub>/ITO flat film and the concaved part of the PDMS stamp. Interdigitated microelectrodes were created when different aqueous etching solutions passed through the microfluidic channel to etch MnO<sub>2</sub> and ITO successively. Etching rate was time dependent. Close control of exposure time to etching solution followed by immediate washing is required to prevent diffusion of etchant into the unexposed materials. The PDMS stamp used is cheap and stable against a wide range of the etchants, making the microfluidic etching a fast and cost-effective method for electrode patterning.

#### 2.4. Direct Printing of Patterned Active Electrodes

Direct printing of active materials is a simple and cost-effective alternative approach to fabricate interdigitated electrodes, which can avoid the unnecessary waste of materials and enable asymmetric design of fMSCs. Different to other approaches, the printing approach aims to transfer the existing electrode material in ink solution onto a substrate in the form of interdigitated microelectrodes. Various printing techniques, including screen printing,<sup>[77]</sup> gravure printing,<sup>[78]</sup> inkjet printing,<sup>[79]</sup> and



extrusion printing,<sup>[80]</sup> have been exploited to prepare fMSC electrodes. While these printing techniques are mature and have been widely used in industry, the development of printable inks which contain active materials suitable for fMSC that are compatible with these deposition technologies is still a main challenge.

#### 2.4.1. Conventional Printing Techniques: Screen Printing and Gravure Printing

Screen printing and gravure printing are two conventional printing techniques, which require a prepatterned mediator (i.e., screen and carved cylinder) for the definition of electrode patterns and slurry-like viscous inks.

In screen printing, the ink is forced through a screen with prepatterned open meshes and the pattern is left on a substrate. To achieve a printable ink, active materials are usually dispersed together with a polymer binder (e.g., PVDF) in an appropriate solvent to a desired slurry feature. Polymer binders can increase the viscosity of inks and also help form a continuous feature of printed active materials rather than distributed particle dots. Wang et al. fabricated a  $\text{MnO}_2$ /onion-like carbon ( $\text{MnO}_2$ /OLC)-based fMSCs by screen printing  $\text{MnO}_2$ /OLC-based ink (Figure 10a).<sup>[77]</sup> In this work, a layer of silver (Ag) conductive paint was first printed onto the PET substrate, to act as the current collector of a fMSC. Subsequently, the slurry-like ink containing 80 wt% active materials of  $\text{MnO}_2$ /OLC, 10 wt% conductive carbon black and 10 wt% PVDF binder in *N*-methyl pyrrolidone (NMP) were printed on top of the Ag electrode, followed by drying at 110 °C in an oven. The printed microelectrode showed a uniform thickness of 10  $\mu\text{m}$  and the fabricated fMSC device exhibited an areal capacitance of 7.04  $\text{mF cm}^{-2}$  and a volumetric capacitance of 7.04  $\text{F cm}^{-3}$ .

Following a similar procedure, Yang and co-workers prepared a fMSC based on cobalt oxide (CoO)/CNT 3D nanocomposites, in which CoO nanoflowers were woven within the CNT networks.<sup>[81]</sup> High capacitances of 17.4  $\text{mF cm}^{-2}$  and 17.4  $\text{F cm}^{-3}$  were achieved due to the advanced morphology of active materials. A nitrogen-doped graphene-based fMSC with electrode thickness of 10  $\mu\text{m}$  has also been screen-printed, which delivered an areal capacitance of 3.4  $\text{mF cm}^{-2}$ .<sup>[82]</sup>

Gravure printing is a traditional roll-to-roll technique for the printing of newspapers, magazines, and packages. In this approach, image elements are carved into the surface of a cylinder, and the carved area is flooded with ink when the cylinder goes through an ink fountain. Reservoir ink is then transferred onto the substrate by the high printing pressure and adhesive forces between the ink and substrate.<sup>[83]</sup> To prepare a printable ink, volatile solvents (e.g., ethanol or water) are used to disperse active materials and the viscosity of the ink is typically in the range of 0.05–0.2 Pa s to ensure proper loading and transfer of the ink onto the substrate. Shi and co-workers fabricated a fMSC by gravure printing based on hybrid  $\text{MoS}_2$ @S-rGO, which is a highly porous material consisting of sulfonated reduced graphene oxide (S-rGO) and  $\text{MoS}_2$  nanoflowers (Figure 10b).<sup>[78]</sup> In their work, the water/ethanol-based hybrid  $\text{MoS}_2$ @S-rGO with ink viscosity of 0.5 Pa s was printed to an interdigitated pattern onto an  $\text{O}_2$  plasma-treated hydrophilic PI substrate. The fabricated fMSC device delivered a high areal capacitance of 6.56  $\text{mF cm}^{-2}$  and a volumetric capacitance of 4.37  $\text{F cm}^{-3}$ . Chen and co-workers dispersed a template-assisted graphene into a volatile solvent system (water:ethanol = 4:1) at a high solid content concentration of 133  $\text{mg mL}^{-1}$ .<sup>[83]</sup> The ink was repeatedly printed on PI sheets for 20 layers to achieve an electrode thickness of 10  $\mu\text{m}$ . High areal and volumetric capacitances of 6.65  $\text{mF cm}^{-2}$  and 6.65  $\text{F cm}^{-3}$ , respectively, were achieved by the fabricated device. Despite the fast and

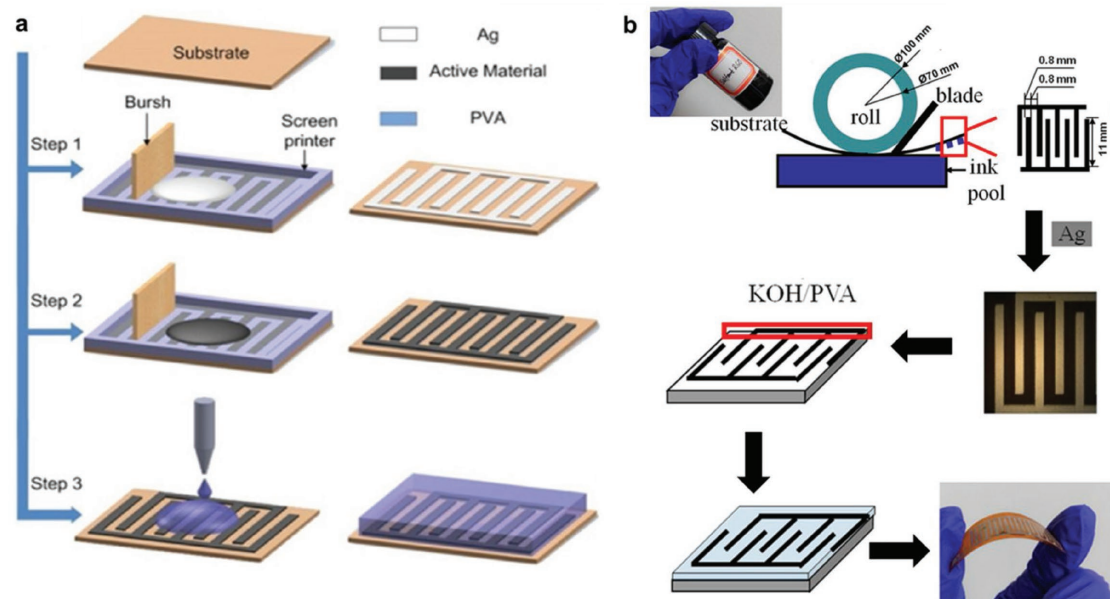


**Figure 10.** Schematic diagram of the fabrication process via a) screen printing and b) gravure printing techniques. a) Reproduced with permission.<sup>[77]</sup> Copyright 2014, IOP Publishing Ltd., and b) reproduced with permission.<sup>[78]</sup> Copyright 2015, AIP Publishing LLC.

cost-effective process of the abovementioned printing techniques, the poor resolution ( $\approx 300\ \mu\text{m}$  for screen printing and  $\approx 700\ \mu\text{m}$  for gravure printing) limited the performance of the final fMSC device.<sup>[78]</sup>

#### 2.4.2. Inkjet Printing

Inkjet printing is a digital and noncontact technology, which prints more precise patterns without the use of a prepatterned intermediate carrier.<sup>[84]</sup> In the inkjet printing process, the print head is controlled by an XY-motor and the printed pattern can be changed and modified using simple CAD software. The process involves continuously generating droplets (10–20 pL) and catapulting them out of a thin nozzle (typical size of 20–30  $\mu\text{m}$  in inner diameter) by heat or piezo effect. These conditions require specific ink stability and particle size. A typical low viscosity of less than 20 mPa s and a surface tension ranging from 28 to 350 mN m<sup>-1</sup> are also required for continuous droplet formation.<sup>[85]</sup> Strategies to achieve printable inks include the addition of polymer additives or surfactants to disperse active materials well and the use of mixed solvent systems to achieve the required surface tension.<sup>[84]</sup>

For example, Hersam and co-workers prepared a graphene-based ink for inkjet printing via dispersing graphene together with a polymer additive of ethyl cellulose (EC) in a 85:15 solvent mixture of cyclohexanone/terpineol.<sup>[79]</sup> The stable ink has a suitable surface tension of  $\approx 33\ \text{mN m}^{-1}$  and a high shear rate (100–1000 s<sup>-1</sup>) viscosity of 10–12 mPa s at a graphene concentration of 3.4 mg mL<sup>-1</sup>. The fMSC device fabricated from the inkjet-printed interdigitated electrodes delivered a high volumetric capacitance of 9.3 F cm<sup>-3</sup>. However, due to the ultrathin graphene thickness of 40 nm, the device exhibited a low areal capacitance of 37.2  $\mu\text{F cm}^{-2}$ . As an additive printing technology, the loading and thickness of active materials can be increased via repeatedly printing layer upon layer to achieve higher areal capacitance. Östling and co-workers dispersed electrochemically exfoliated graphene using the same procedure (i.e., using EC as stabilizer in cyclohexanone/terpineol solvent system).<sup>[86]</sup> Thicker interdigitated electrodes (with thickness up to  $\approx 0.7\ \mu\text{m}$ ) were printed and the device delivered a higher areal capacitance of 0.7 mF cm<sup>-2</sup>. They also demonstrated the scalability of this technique by printing 12 series  $\times$  12 parallel devices on a flexible PI substrate.

Inkjet printing has the potential to print every component in a fMSC device. Lee and co-workers developed an all-inkjet-printed fMSC on paper by successively printing the current collectors,

electrode materials, and electrolyte (**Figure 11**).<sup>[87]</sup> The current collector ink was prepared by dispersing AgNWs in water/isopropanol in which the AgNWs were sonicated to avoid clogging of nozzles. An aqueous ink of electrode materials containing single-walled carbon nanotube (SWNT)/activated carbon (AC) and sodium dodecylbenzene sulfonate (SDBS) acting as dispersing agent was subjected to high speed centrifugation to remove large-sized particles and agglomerates. A printable and UV curable gel electrolyte of 1-butyl-3-methylimidazolium tetrafluoroborate ([BMIM][BF<sub>4</sub>])/ethoxylated trimethylolpropane triacrylate (ETPTA) was also printed and UV irradiated to form a crosslinked solid-state polymer electrolyte. This strategy opened up a new way for the fabrication of fMSCs and the application in next-generation fully printed wearable electronics.

Inkjet printing also allows for the fabrication of asymmetric fMSCs. As reported by Huang and co-workers, a pseudocapacitive K<sub>2</sub>Co<sub>3</sub>(P<sub>2</sub>O<sub>7</sub>)<sub>2</sub>·2H<sub>2</sub>O nanocrystal whiskers' ink and a graphene ink in ethanol were printed as the positive and negative materials, respectively.<sup>[88]</sup> Minimum microelectrode widths of 70 and 80  $\mu\text{m}$  on the positive and negative electrodes without shorting the circuit can be achieved. The assembled device with 1.07 V operating voltage window delivered a high capacitance of 6 F cm<sup>-3</sup> and a maximum energy density of 0.96 mWh cm<sup>-3</sup>. The potential in scalable fabrication, fully printed devices, and asymmetric fMSCs has made inkjet printing promising. However, the processing efficiency is still low due to the low solid concentration of inks (to ensure compatibility with the inkjet process).

#### 2.4.3. Extrusion Printing

Extrusion printing, which involves extruding a viscous ink through a nozzle mounted on a XYZ-positioning stage, is considered to be a scalable patterning technique to prepare fMSCs with high loading level of active materials.<sup>[89–91]</sup> Similar to inkjet printing, the printed pattern in extrusion printing is controlled via software on a computer and allows freedom in design of pattern parameters. However, extrusion printing has different requirements on the rheology properties of stable inks. An ink which shows high viscosity at a low shear rate is desirable because the high viscosity prevents the ink from immediately spreading on the substrate and thus can form constant lines along the movement direction of the nozzle as extruded. A good flowability at printing shear rate is also required to make sure that the ink can easily flow through the printing nozzles under the applied pressure, thus a shear thinning behavior of the ink is favorable.<sup>[89–91]</sup>

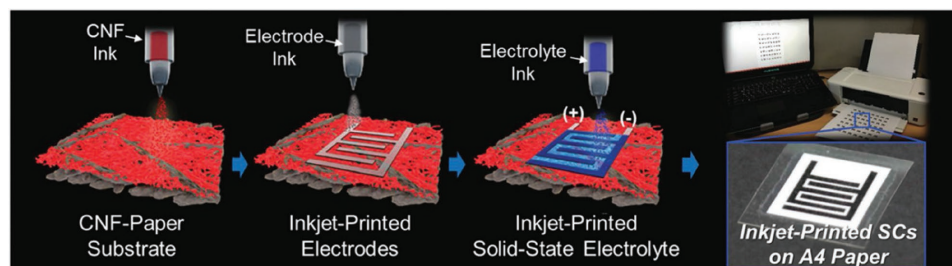


**Figure 11.** Schematic illustration of the stepwise fabrication procedure of the inkjet-printed SCs, and a photograph of the desktop inkjet printer used herein. Reproduced with permission.<sup>[87]</sup> Copyright 2016, Royal Society of Chemistry.

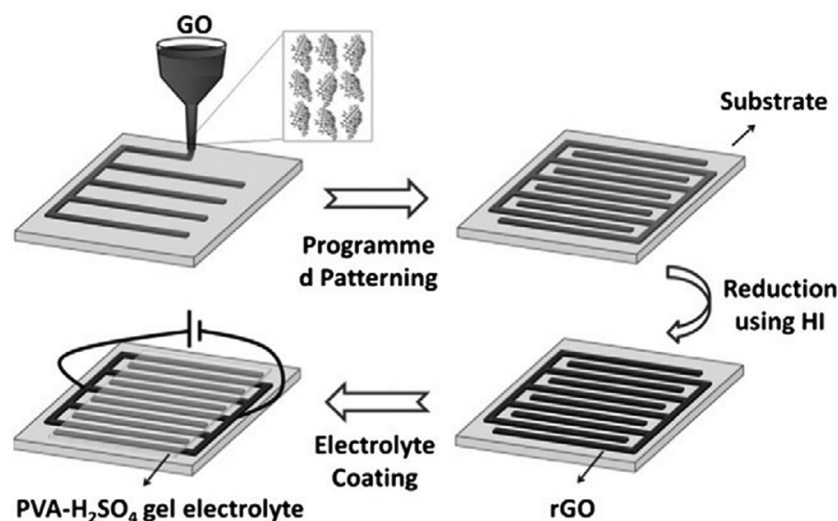


**Figure 12.** Schematic illustration of device fabrication via extrusion printing technique. Reproduced with permission.<sup>[80]</sup> Copyright 2015, Elsevier Ltd.

Aqueous dispersions of GO typically display concentration dependent shear thinning behavior, which suggest remarkable printing capabilities.<sup>[92]</sup> Sun et al. used a viscous and concentrated GO solution ( $20 \text{ mg mL}^{-1}$ ) ink and extrusion-printed interdigitated microelectrodes with electrode width and interspacing of  $\approx 600$  and  $\approx 500 \text{ }\mu\text{m}$ , respectively, after which the GO pattern was chemically reduced and electrolyte coating was applied (Figure 12).<sup>[80]</sup> The thickness and areal capacitance can be readily scaled from  $1.04$  to  $\approx 4$  and  $\approx 3$  to  $19.8 \text{ mF cm}^{-2}$  via repeated layer-by-layer printing (from 1 to 4 layers). Ding and co-workers developed an extrusion-printed CNT-based fMSC with high resolution ( $235.7 \text{ }\mu\text{m}$  width and  $185 \text{ }\mu\text{m}$  interspacing) using with a small diameter nozzle ( $60 \text{ }\mu\text{m}$ ).<sup>[93]</sup> The ink was prepared by dispersing CNTs with a commercial dispersion agent in isopropanol at a high CNT concentration of  $80 \text{ mg mL}^{-1}$ , which possess apparent shear thinning behavior and a relatively high viscosity of  $0.2 \text{ Pa s}$  at  $1 \text{ s}^{-1}$ . An areal capacitance of  $2.5 \text{ mF cm}^{-2}$  was achieved by a 5-layer printed CNT fMSC. Despite that the asymmetric fMSCs have not been fabricated via extrusion printing technology, some Li-ion microbatteries which have different materials in anode and cathode have been fabricated via extrusion printing of anode and cathode inks.<sup>[92,94]</sup> It is highly likely that the technology can be directly transferred to produce asymmetric fMSCs.

In general, although digital printing techniques including inkjet printing and extrusion printing having high requirements on ink properties including particle size, concentration, viscosity, and rheology behavior, they are superior to screen printing and gravure printing in terms of the following merits: 1) they offer easy control on the thickness of electrodes via layer-by-layer printing, which is a good way to enhance the areal capacitance; 2) they allow freedom of achieving desired patterns such as the width and length of microelectrodes, as well as the series/parallel connections between single devices; 3) asymmetric microelectrodes (different materials for the positive and negative materials) can be individually printed, which are difficult to obtain by other techniques; 4) since printable gel electrolytes have been developed recently and some packaging

materials (like PDMS) are printable, this technology enables the fully printed device fabrication and simplifies fabrication steps. In addition, digital printing of other micro-electronics is becoming a promising field. Cofabrication using the same processing techniques will further simplify production of micro-supercapacitors and external electronics. Therefore, inkjet printing and extrusion printing are the most promising techniques in the fabrication of interdigitated microelectrodes and further efforts should be paid in producing the compatible inks.

## 2.5. Summary of Fabrication Approaches

fMSCs are a promising candidate to be integrated with functional devices for self-powered wearable electronics due to their special in-plane interdigitated electrode architecture. With rational design of active

materials, electrolyte, and device architectures, fMSCs are expected to provide efficient energy and high power to replace or supplement microbatteries. As stated above, several representative strategies have been proposed for the fabrication of fMSCs. Although these methods show great potential, they still have their own limitations. Photolithography is widely used in microelectronics manufacturing at nanometer resolution. It is an excellent fabrication process to control the interspace between interdigitated microelectrodes which determines the performance of the device. However, it often involves complicated and time consuming processes, toxic etchant treatment and needs an ultraclean environment. Laser writing is facile, fast, and ready for scalable production. Electrode fabrication and patterning are done simultaneously, but it is only suitable for specific materials. Etch patterning requires thin film preparation in advance, and the film thickness should be well controlled to make sure that etching can be fully achieved. Printing technologies are capable of directly printing active materials into interdigitated patterns on flexible substrates. The challenge for this method is the preparation of stable inks with suitable rheological properties. The comparison of these fabrication strategies are summarized in Table 1.

## 3. Integration

As an important energy storage unit, the rational integration with other components in an electric circuit is crucial for fMSCs. Efforts have been made to integrate flexible SCs with sandwiched structures into wearable electronics to store energy from sustainable and renewable energy harvesting units (e.g., solar cells<sup>[95,96]</sup> and nanogenerators<sup>[97]</sup>) and deliver power to electronic devices (e.g., LED,<sup>[98]</sup> timer,<sup>[99]</sup> photodetector,<sup>[100]</sup> and sensors<sup>[101,102]</sup>). In addition, series and/or parallel connection between several single SCs are made in some applications where the current or voltage requirement is higher than what a single SC device can deliver. However, the use of



**Table 1.** Comparison of different fabrication strategies for fMSCs.

Fabrication strategy		Active materials	Device configurations	Possibility for large-scale fabrication	Fabricating precision
Deposition of active materials on prepatterned current collectors	Photolithograph	Carbons, CPs <sup>a)</sup> , MOs <sup>b)</sup>	Symmetric, asymmetric	No	High
	Mask			Yes	Medium
Laser writing		Graphene, graphene/MO	Symmetric, asymmetric	Yes	Medium
Etching patterning	Plasma etching	Carbons, CPs, MOs	Symmetric	No (for mask involved) Yes (for micro-plasma jet)	High
	Laser etching			Yes	
	Microfluidic etching			No	
Direct printing	Conventional printing (screen printing and gravure printing)	Carbons, MOs	Symmetric	Yes	Medium
	Inkjet printing	Carbons, CPs, MOs	Symmetric, asymmetric		High
	Extrusion printing	Carbons	Symmetric, asymmetric		High

<sup>a)</sup>CPs: conducting polymers; <sup>b)</sup>MOs: metal oxides.

intricate connecting wires makes the electronic system bulky and heavy, which make them unsuitable in miniaturized wearable microelectronics. The in-plane interdigitated structure of fMSCs, which has both electrodes on the same plane, has the potential to be integrated with other components or connected in series or parallel on a substrate via embedded conducting lines (e.g., liquid metal lines) within a limited footprint. The whole integrated system is therefore small, lightweight, robust, and suitable in wearable applications. In addition, fMSCs with unique interdigitated electrode structure exhibit high power density ( $>1 \text{ mW cm}^{-2}$ ),<sup>[103]</sup> which is sufficient for most of the wearable applications (in the scale of microwatts).<sup>[5]</sup> Great achievements have been obtained in energy density of fMSCs in the range of  $0.01\text{--}100 \text{ } \mu\text{Wh cm}^{-2}$  during the past few years (Figure 13).<sup>[9,11,13,19,50,55,72,74,75,104–111]</sup> And, some successful integrated systems have been achieved with fMSCs.

For example, Xu and Shen designed a highly integrated self-driven on-chip photodetector by integrating a rGO-based fMSC with a photoresponing CdS nanowire material.<sup>[31]</sup> In the system, a square-shaped gold electrode was made in between two electrodes of rGO-fMSC, connecting to one fMSC electrode by printed CdS nanowires. A photodetector was formed consisting of the current collector (Au) on the fMSC electrode as one electrode and the middle square-shaped gold electrode as another electrode. With the charged fMSC providing a voltage between two electrodes, the photodetector has high photocurrent response when illuminated by white light and no current response in dark. The photodetector driven by fMSC exhibited stable photocurrent response, consistent with the same device but driven by the external power source (0.32 V), indicating the feasibility of flexible integrated system. A series of fMSC arrays can also be facily attached or directly fabricated onto an energy harvesting unit to store energy. They also developed an integrated wearable gas sensing system and electronic skins powered by fMSCs.<sup>[32,102]</sup> A typical example is the flexible self-charging MSC power unit (SCMPU) fabricated by Wang and co-workers.<sup>[112]</sup> In this system, four series-connected laser-induced graphene (LIG) fMSCs were fabricated on the back of a triboelectric nanogenerator (TENG) (Figure 14a), and

storage charges generated from the TENG through contact electrification and electrostatic induction. The SCMPU system is flexible and small, which made it easy to be inserted into the insole of a shoe (Figure 14c) and harvest energy during walking. The fully charged SCMPU unit is powerful enough to light two LEDs and supply power for a commercial hygromograph, demonstrating its potential in wearable application.

In recent years, research on body-attached sensing devices, which are fabricated on a stretchable, biocompatible, and skin-attachable PDMS substrate, has been extensively conducted to monitor body health and environmental conditions.<sup>[113]</sup> These advances have imposed pressure on the development of integrable power supply devices that have stable performance

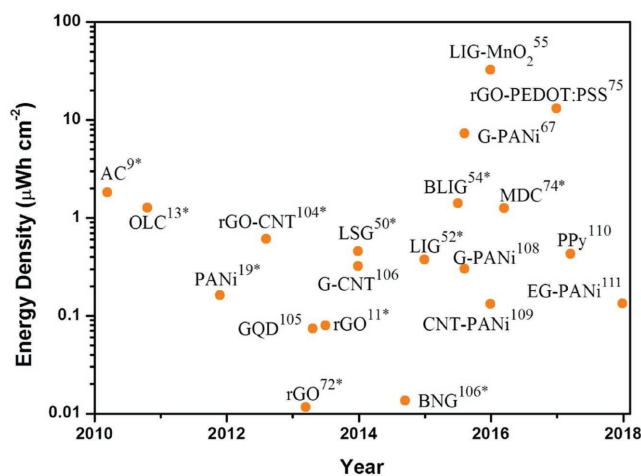


**Figure 13.** Energy density of the fMSC devices reported over the past years (calculated based on the area of the whole device). \*Calculated based on the dimensions given in reference when specific results were not given. AC, activated carbon; BLIG, boron-doped laser-induced graphene; BNG, boron, nitrogen-doped graphene; CNT, carbon nanotube; EG, exfoliated graphene; G, graphene; GQD, graphene quantum dot; LIG, laser-induced graphene; LSG, laser-scribed graphene; MDC, mushroom derived carbon; OLC, onion-like carbon; PANi, polyaniline; PPy, polypyrrole; PEDOT:PSS, poly(3,4-ethylenedioxythiophene): poly(styrenesulfonate); rGO, reduced graphene oxide.

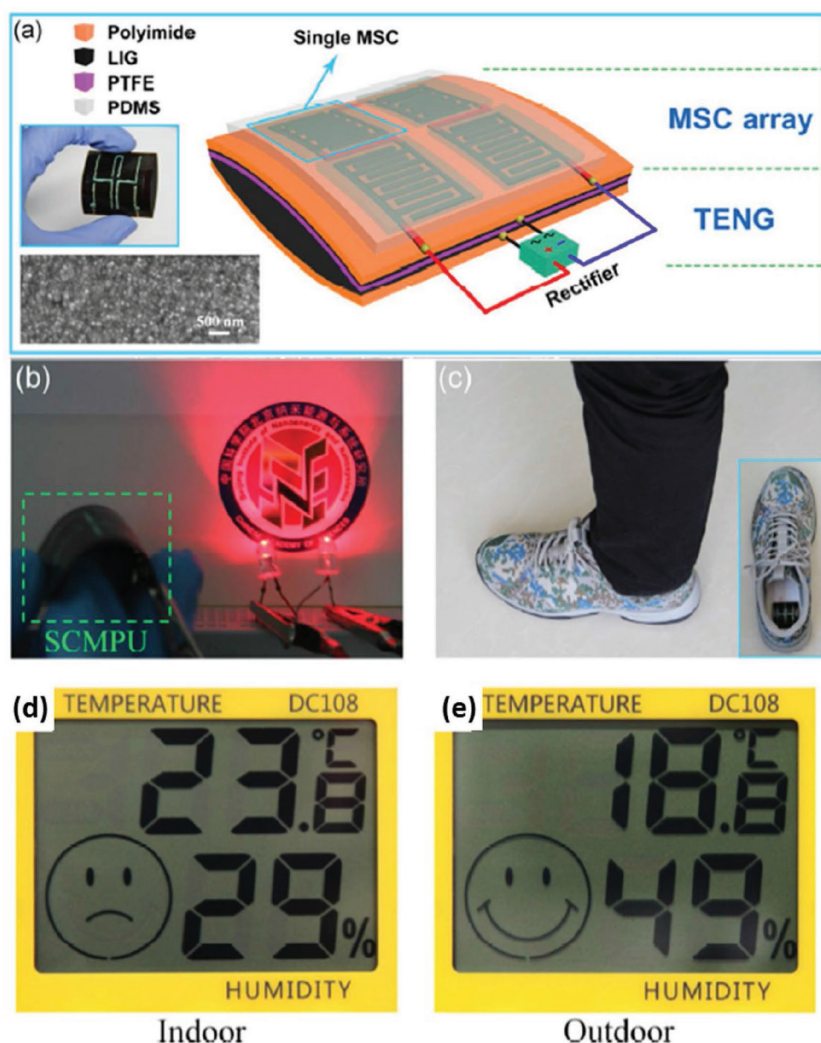


**Figure 14.** a) Schematic depicting the detailed structure of the SCMPU. Top inset: photograph of SCMPU; bottom inset: SEM image of PTFE nanoparticles applied onto the surface of PTFE film. b) Photograph showing two LEDs being powered by the SCMPU. c) Photograph of the SCMPU inserted in the insole of a shoe. d,e) Photographs of using the SCMPU to drive a commercial hygrothermograph. All panels reproduced with permission.<sup>[112]</sup> Copyright 2015, Springer.

under deformation due to body movement. The miniaturized fMSCs can meet these requirements. In the work of Ha and co-workers, a series of CNT-based fMSC (on PET film) arrays

were implanted into soft PDMS substrate (Ecoflex silicone elastomer), and connected via embedded liquid metal interconnection and Ag nanowire contacts.<sup>[114]</sup> These fMSC arrays can maintain stable electrochemical performance under 100% uniaxial and 50% biaxial stretching and light LED arrays under strain conditions. This work indicated the potential application of the stretchable fMSC arrays to wearable and body-attachable electronics with a self-powered system. To demonstrate the real applications of these stretchable fMSC arrays, stretchable multisensing system operated by these fMSC arrays was developed.<sup>[115]</sup> In this work, an array of nine CNT-based fMSCs, individual sensors (a fragmented graphene foam strain sensor and a MWNT/SnO<sub>2</sub>-based NO<sub>2</sub>/UV sensor), and a wireless radio frequency (RF) power receiver were transferred onto a flexible and biocompatible silicon Ecoflex substrate, and connected by embedded liquid metal lines (Figure 15). The fabricated system could be attached to the skin and successfully detect biosignals, such as a neck pulse, saliva swallowing, voice and body movements and could provide a stable sensing signal upon exposure to NO<sub>2</sub> gas and UV light under a uniaxial strain up to 50%. Although further improvements like pursuing higher output voltage of fMSC arrays and exploring matching components are still required, this work shows the great potential of fMSCs in the next-generation next-to-skin healthcare and environmental sensing systems.

## 4. Prospects

fMSCs play a crucial role as energy storage devices for the next-generation miniaturized wearable electronics, so the facile fabrication of high-performance fMSCs in the large-scale is of great importance. Efforts in the following aspects can be paid to expedite the further advancement of fMSCs.

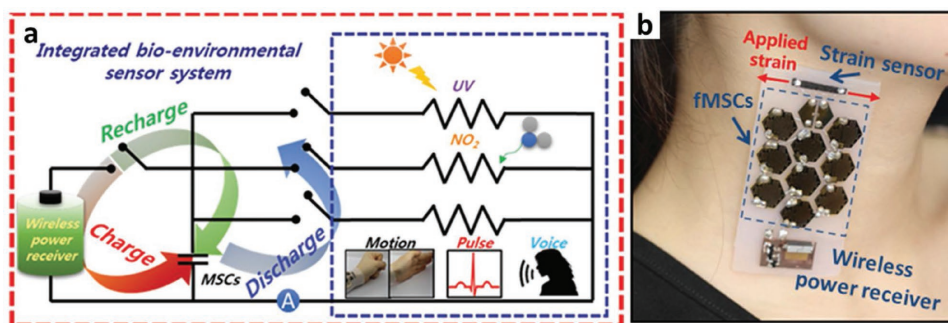


**Figure 15.** a) Circuit diagram of an integrated system. b) Photograph of a fragmented graphene foam (FGF) sensor attached on the skin of a neck. All panels reproduced with permission.<sup>[115]</sup> Copyright 2016, Wiley-VCH.

Developing engineering processable electrode materials with high performance which can fit one of the abovementioned patterning techniques is crucial. Since the largest number of fMSCs is made from carbon-based materials, the proper incorporation of highly capacitive pseudocapacitive materials (including PANi, Ppy, MnO<sub>2</sub>, RuO<sub>2</sub>, etc.) and the new generation of advanced materials (like NiCo<sub>2</sub>S<sub>4</sub>, metal–organic frameworks (MOFs), Mxene, etc.) into the processable nanostructured carbon materials is demanded to improve the energy and power density of fMSCs.

The optimization of geometric parameters including the interspace, width, length, and numbers of microelectrodes is needed to be improved in the design of future flexible interdigitated MSCs. The effects of varying the width and the interspace between electrode fingers have been investigated in previous reports.<sup>[70]</sup> Liu et al. fabricated electrode fingers with different interspace widths on the same total surface of cell. They found that volumetric specific capacitance decreased with increase of the interspace width. This can be ascribed to the different routes for ion diffusion from the electrolyte to the surface of electrodes. Larger width of interspace between adjacent electrode fingers leads to a longer average ionic diffusion pathway. The effect of the width of electrode fingers was also evaluated by keeping the interspace width, the length of the fingers, and the thickness constant. It was found that the performance of MSCs could be enhanced by reducing the width of electrode fingers. Narrow fingers maximized the accessible surface area of electrodes and resulted in improved capacitance. It should be noted that the electric field distribution should be taken into account, since when the interspace is too narrow, the electric field might be too strong to breakdown the electrolyte, resulting in electric leakage and short circuit. Therefore, an appropriate interspace, width, and length of electrode fingers should be chosen to fabricate high performance flexible interdigitated MSCs. Geometries other than simple interdigitated design should also be considered for in-plane fMSCs. In a recent report, Alshareef and co-workers fabricated MSCs using Hilbert, Peano, and Moore fractal electrode designs. The MSCs based on the Moore design showed a 32% enhancement in energy density compared to conventional interdigitated structures, while maintaining the same power density when using the same thin-film electrodes. They also proposed that the increase in electric lines of force caused by the edging effect in the fractal electrodes also contributed to the enhanced capacitance.<sup>[17]</sup>

The development of simple, low-cost, high-throughput techniques for microelectrode fabrication is in high demand to realize large-scale production of fMSCs for wearable electronics. To meet this requirement, active materials should be deposited on the flexible substrate directly without the preparation and postpatterning of thin film. Digital printing techniques (including inkjet printing and extrusion printing) possess the most advantages in microelectrode fabrication due to their simplicity in industrial-level fabrication and the high degree of flexibility in the patterns and geometries. Meanwhile, it is promising to realize asymmetric fMSCs, fully printed fMSCs devices, the cofabrication and integration of fMSCs with other printable electronics components. Therefore, efforts should be paid to the preparation of printable ink formulations

which are composed of active materials (especially containing pseudocapacitive materials), polymer gel electrolytes, current collectors, electrical conducting lines, and packaging materials.

Due to the rapid development in wearable functional devices, such as strain sensors, pressure sensor, and e-skins, MSCs that are not only flexible but also stretchable are expected. Ha and co-workers fabricated stretchable MSC arrays by using liquid metal interconnects.<sup>[115]</sup> The stretchable MSC arrays were sufficient to power integrated strain and gas sensors. Another efficient way to fabricate stretchable MSCs is to design out-of-plane wavy electrodes. Chen and co-workers fabricated stretchable MSCs with suspended wavy electrodes.<sup>[116]</sup> The strain applied to the device is compensated by the deformation of wavy structures rather than on the electrode itself. Shen and co-workers prepared a stretchable MSC on PDMS with wavy channels which was cured on a 3D-printed mold with convex electrodes.<sup>[35]</sup> MSCs with intrinsic stretchability are still under development to achieve higher strain tolerance while keeping stable electrochemical performance. Therefore, more attention should be paid to the construction of intrinsically stretchable MSCs to be integrated with stretchable electronics as power sources. We believe that with the rapid development of materials science and fabrication techniques, all of these issues can be addressed in the near future.

## Acknowledgements

C.Z. and Y.L. contributed equally to this work. Funding from the Australian Research Council Centre of Excellence Scheme (CE 140100012) and Australian National Fabrication Facility (Materials node) are gratefully acknowledged. J.C. and J.R. gratefully acknowledge the ARC for support under the Discovery Project (DP170102320) and the Future Fellowship (FT130100380) schemes, respectively. Y.L. would like to acknowledge the support of the CSC scholarship from the Ministry of Education of P. R. China. C.Z. would like to thank the financial support from the Start-Up research grant of Guangdong University of Technology (220413181), and the Program for Guangdong Introducing Innovative and Entrepreneurial Teams (2016ZT06C412).

## Conflict of Interest

The authors declare no conflict of interest.

## Keywords

fabrication, micro-supercapacitor, wearable devices

Received: January 23, 2018

Revised: March 7, 2018

Published online: June 19, 2018

[1] Z. L. Wang, *Nano Today* **2010**, 5, 512.

[2] Z. L. Wang, *Adv. Mater.* **2012**, 24, 280.

[3] Z. L. Wang, W. Wu, *Angew. Chem., Int. Ed.* **2012**, 51, 11700.

[4] J. W. Long, B. Dunn, D. R. Rolison, H. S. White, *Chem. Rev.* **2004**, 104, 4463.

[5] M. Beidaghi, Y. Gogotsi, *Energy Environ. Sci.* **2014**, 7, 867.



- [6] J. Yan, Q. Wang, T. Wei, Z. Fan, *Adv. Energy Mater.* **2014**, 4, 1300816.
- [7] Y. Wang, Y. Xia, *Adv. Mater.* **2013**, 25, 5336.
- [8] P. Simon, Y. Gogotsi, *Nat. Mater.* **2008**, 7, 845.
- [9] D. Pech, M. Brunet, P.-L. Taberna, P. Simon, N. Fabre, F. Mesnilgrete, V. Conédéra, H. Durou, *J. Power Sources* **2010**, 195, 1266.
- [10] H. Ben, M. Julian, W. Shuang, I. Jung Bin, C. Carlo, P. Dimos, P. G. Costas, M. Roy, *Nanotechnology* **2014**, 25, 055401.
- [11] Z. Niu, L. Zhang, L. Liu, B. Zhu, H. Dong, X. Chen, *Adv. Mater.* **2013**, 25, 4035.
- [12] Z.-S. Wu, K. Parvez, X. Feng, K. Mullen, *J. Mater. Chem. A* **2014**, 2, 8288.
- [13] D. Pech, M. Brunet, H. Durou, P. Huang, V. Mochalin, Y. Gogotsi, P.-L. Taberna, P. Simon, *Nat. Nanotechnol.* **2010**, 5, 651.
- [14] J. Chmiola, C. Largeot, P.-L. Taberna, P. Simon, Y. Gogotsi, *Science* **2010**, 328, 480.
- [15] W. Si, C. Yan, Y. Chen, S. Oswald, L. Han, O. G. Schmidt, *Energy Environ. Sci.* **2013**, 6, 3218.
- [16] L. Peng, X. Peng, B. Liu, C. Wu, Y. Xie, G. Yu, *Nano Lett.* **2013**, 13, 2151.
- [17] M. K. Hota, Q. Jiang, Y. Mashraei, K. N. Salama, H. N. Alshareef, *Adv. Electron. Mater.* **2017**, 3, 1700185.
- [18] C. Meng, J. Maeng, S. W. M. John, P. P. Irazoqui, *Adv. Energy Mater.* **2014**, 4, 1301269.
- [19] K. Wang, W. Zou, B. Quan, A. Yu, H. Wu, P. Jiang, Z. Wei, *Adv. Energy Mater.* **2011**, 1, 1068.
- [20] J.-H. Sung, S.-J. Kim, K.-H. Lee, *J. Power Sources* **2003**, 124, 343.
- [21] N. Kurra, M. K. Hota, H. N. Alshareef, *Nano Energy* **2015**, 13, 500.
- [22] D. Qi, Y. Liu, Z. Liu, L. Zhang, X. Chen, *Adv. Mater.* **2017**, 29, 1602802.
- [23] X. Lu, M. Yu, G. Wang, Y. Tong, Y. Li, *Energy Environ. Sci.* **2014**, 7, 2160.
- [24] Y. Yin, C. Liu, S. Fan, *J. Phys. Chem. C* **2012**, 116, 26185.
- [25] X. Cai, M. Peng, X. Yu, Y. Fu, D. Zou, *J. Mater. Chem. C* **2014**, 2, 1184.
- [26] H. Hu, Z. Pei, C. Ye, *Energy Storage Mater.* **2015**, 1, 82.
- [27] J. J. Yoo, K. Balakrishnan, J. Huang, V. Meunier, B. G. Sumpter, A. Srivastava, M. Conway, A. L. Mohana Reddy, J. Yu, R. Vajtai, P. M. Ajayan, *Nano Lett.* **2011**, 11, 1423.
- [28] X. Peng, L. Peng, C. Wu, Y. Xie, *Chem. Soc. Rev.* **2014**, 43, 3303.
- [29] Z.-S. Wu, X. Feng, H.-M. Cheng, *Natl. Sci. Rev.* **2014**, 1, 277.
- [30] Y. Han, Y. Ge, Y. Chao, C. Wang, G. G. Wallace, *J. Energy Chem.* **2018**, 27, 57.
- [31] J. Xu, G. Shen, *Nano Energy* **2015**, 13, 131.
- [32] L. Li, C. Fu, Z. Lou, S. Chen, W. Han, K. Jiang, D. Chen, G. Shen, *Nano Energy* **2017**, 41, 261.
- [33] H. Hu, Z. Pei, H. Fan, C. Ye, *Small* **2016**, 12, 3059.
- [34] Y.-Y. Peng, B. Akuzum, N. Kurra, M.-Q. Zhao, M. Alhabeb, B. Anasori, E. C. Kumbur, H. N. Alshareef, M.-D. Ger, Y. Gogotsi, *Energy Environ. Sci.* **2016**, 9, 2847.
- [35] L. Li, Z. Lou, W. Han, D. Chen, K. Jiang, G. Shen, *Adv. Mater. Technol.* **2017**, 2, 1600282.
- [36] W. Liu, C. Lu, H. Li, R. Y. Tay, L. Sun, X. Wang, W. L. Chow, X. Wang, B. K. Tay, Z. Chen, J. Yan, K. Feng, G. Lui, R. Tjandra, L. Rasenthiram, G. Chiu, A. Yu, *J. Mater. Chem. A* **2016**, 4, 3754.
- [37] R. Z. Li, R. Peng, K. D. Kihm, S. Bai, D. Bridges, U. Tumuluri, Z. Wu, T. Zhang, G. Compagnini, Z. Feng, A. Hu, *Energy Environ. Sci.* **2016**, 9, 1458.
- [38] X. Pu, M. Liu, L. Li, S. Han, X. Li, C. Jiang, C. Du, J. Luo, W. Hu, Z. L. Wang, *Adv. Energy Mater.* **2016**, 6, 1601254.
- [39] X. Wang, X. Lu, B. Liu, D. Chen, Y. Tong, G. Shen, *Adv. Mater.* **2014**, 26, 4763.
- [40] N. Liu, Y. Gao, *Small* **2017**, 13, 1701989.
- [41] L. Li, Z. Lou, D. Chen, K. Jiang, W. Han, G. Shen, *Small* **2017**, 1702829, <https://doi.org/10.1002/sml.1702829>.
- [42] T. Huang, K. Jiang, D. Chen, G. Shen, *Chin. Chem. Lett.* **2017**, 29, 553.
- [43] J.-H. Sung, S.-J. Kim, S.-H. Jeong, E.-H. Kim, K.-H. Lee, *J. Power Sources* **2006**, 162, 1467.
- [44] D. Kim, G. Lee, D. Kim, J. S. Ha, *ACS Appl. Mater. Interfaces* **2015**, 7, 4608.
- [45] H. Hu, K. Zhang, S. Li, S. Ji, C. Ye, *J. Mater. Chem. A* **2014**, 2, 20916.
- [46] Q. Jiang, N. Kurra, H. N. Alshareef, *Adv. Funct. Mater.* **2015**, 25, 4976.
- [47] S. C. Lee, U. M. Patil, S. J. Kim, S. Ahn, S.-W. Kang, S. C. Jun, *RSC Adv.* **2016**, 6, 43844.
- [48] Y. Zhang, L. Guo, S. Wei, Y. He, H. Xia, Q. Chen, H.-B. Sun, F.-S. Xiao, *Nano Today* **2010**, 5, 15.
- [49] W. Gao, N. Singh, L. Song, Z. Liu, A. L. M. Reddy, L. Ci, R. Vajtai, Q. Zhang, B. Wei, P. M. Ajayan, *Nat. Nanotechnol.* **2011**, 6, 496.
- [50] M. F. El-Kady, R. B. Kaner, *Nat. Commun.* **2013**, 4, 1475.
- [51] J. Y. Hwang, M. F. El-Kady, Y. Wang, L. Wang, Y. Shao, K. Marsh, J. M. Ko, R. B. Kaner, *Nano Energy* **2015**, 18, 57.
- [52] J. Lin, Z. Peng, Y. Liu, F. Ruiz-Zepeda, R. Ye, E. L. G. Samuel, M. J. Yacaman, B. I. Yakobson, J. M. Tour, *Nat. Commun.* **2014**, 5, 5714.
- [53] Z. Peng, J. Lin, R. Ye, E. L. G. Samuel, J. M. Tour, *ACS Appl. Mater. Interfaces* **2015**, 7, 3414.
- [54] Z. Peng, R. Ye, J. A. Mann, D. Zakhidov, Y. Li, P. R. Smalley, J. Lin, J. M. Tour, *ACS Nano* **2015**, 9, 5868.
- [55] L. Li, J. Zhang, Z. Peng, Y. Li, C. Gao, Y. Ji, R. Ye, N. D. Kim, Q. Zhong, Y. Yang, H. Fei, G. Ruan, J. M. Tour, *Adv. Mater.* **2016**, 28, 838.
- [56] J. Cai, C. Lv, A. Watanabe, *J. Mater. Chem. A* **2016**, 4, 1671.
- [57] J. Cai, C. Lv, A. Watanabe, *Nano Energy* **2016**, 30, 790.
- [58] L. Wen, F. Li, H.-M. Cheng, *Adv. Mater.* **2016**, 28, 4306.
- [59] Y. Xu, Z. Lin, X. Huang, Y. Liu, Y. Huang, X. Duan, *ACS Nano* **2013**, 7, 4042.
- [60] A. Laforgue, *J. Power Sources* **2011**, 196, 559.
- [61] X. Li, G. Wang, X. Wang, X. Li, J. Ji, *J. Mater. Chem. A* **2013**, 1, 10103.
- [62] L. Yuan, J. Chen, C. Hu, Y. Tong, J. Zhou, Z. L. Wang, X.-H. Lu, X. Xiao, T. Zhai, J. Dai, F. Zhang, B. Hu, X. Wang, L. Gong, *ACS Nano* **2012**, 6, 656.
- [63] D. Xu, Q. Xu, K. Wang, J. Chen, Z. Chen, *ACS Appl. Mater. Interfaces* **2014**, 6, 200.
- [64] H. Fan, N. Zhao, H. Wang, J. Xu, F. Pan, *J. Mater. Chem. A* **2014**, 2, 12340.
- [65] Z. Xin, T. T. C. Bryan, B. Belén, W. Weiliang, J. Colin, M. S. John, S. G. Patrick, *Nanotechnology* **2009**, 20, 065605.
- [66] P. Zhang, Y. Wang, J. Zang, G. Xin, Y. Yuan, X. Qu, *Carbon* **2012**, 50, 5196.
- [67] Z.-S. Wu, K. Parvez, S. Li, S. Yang, Z. Liu, S. Liu, X. Feng, K. Mullen, *Adv. Mater.* **2015**, 27, 4054.
- [68] H.-C. Huang, C.-J. Chung, C.-T. Hsieh, P.-L. Kuo, H. Teng, *Nano Energy* **2016**, 21, 90.
- [69] M. Q. Xue, Z. Xie, L. S. Zhang, X. L. Ma, X. L. Wu, Y. G. Guo, W. G. Song, Z. B. Li, T. B. Cao, *Nanoscale* **2011**, 3, 2703.
- [70] W. Liu, C. Lu, X. Wang, R. Y. Tay, B. K. Tay, *ACS Nano* **2015**, 9, 1528.
- [71] L. Li, Z. Lou, W. Han, G. Shen, *Nanoscale* **2016**, 8, 14986.
- [72] Z.-S. Wu, K. Parvez, X. Feng, K. Mullen, *Nat. Commun.* **2013**, 4, 2487.
- [73] L. Liu, D. Ye, Y. Yu, L. Liu, Y. Wu, *Carbon* **2017**, 111, 121.
- [74] P. Yadav, A. Basu, A. Suryawanshi, O. Game, S. Ogale, *Adv. Mater. Interfaces* **2016**, 3, 1600057.
- [75] Y. Liu, B. Weng, Q. Xu, Y. Hou, C. Zhao, S. Beirne, K. Shu, R. Jalili, G. G. Wallace, J. M. Razal, J. Chen, *Adv. Mater. Technol.* **2016**, 1, 1600166.
- [76] X. Long, Z. Zeng, E. Guo, X. Shi, H. Zhou, X. Wang, *J. Power Sources* **2016**, 325, 264.
- [77] Y. Wang, Y. Shi, C. X. Zhao, J. I. Wong, X. W. Sun, H. Y. Yang, *Nanotechnology* **2014**, 25, 094010.
- [78] Y. Xiao, L. Huang, Q. Zhang, S. Xu, Q. Chen, W. Shi, *Appl. Phys. Lett.* **2015**, 107, 013906.

- [79] L. Li, E. B. Secor, K.-S. Chen, J. Zhu, X. Liu, T. Z. Gao, J.-W. T. Seo, Y. Zhao, M. C. Hersam, *Adv. Energy Mater.* **2016**, 6, 1600909.
- [80] G. Sun, J. An, C. K. Chua, H. Pang, J. Zhang, P. Chen, *Electrochem. Commun.* **2015**, 51, 33.
- [81] Y. G. Zhu, Y. Wang, Y. M. Shi, J. I. Wong, H. Y. Yang, *Nano Energy* **2014**, 3, 46.
- [82] S. Liu, J. Xie, H. Li, Y. Wang, H. Y. Yang, T. Zhu, S. Zhang, G. Cao, X. Zhao, *J. Mater. Chem. A* **2014**, 2, 18125.
- [83] Q. Zhang, L. Huang, Q. Chang, W. Shi, L. Shen, Q. Chen, *Nanotechnology* **2016**, 27, 105401.
- [84] B. J. deGans, P. C. Duineveld, U. S. Schubert, *Adv. Mater.* **2004**, 16, 203.
- [85] B. Weng, R. L. Shepherd, K. Crowley, A. J. Killard, G. G. Wallace, *Analyst* **2010**, 135, 2779.
- [86] J. Li, S. Sollami Delekta, P. Zhang, S. Yang, M. R. Lohe, X. Zhuang, X. Feng, M. Östling, *ACS Nano* **2017**, 11, 8249.
- [87] K.-H. Choi, J. Yoo, C. K. Lee, S.-Y. Lee, *Energy Environ. Sci.* **2016**, 9, 2812.
- [88] H. Pang, Y. Zhang, W.-Y. Lai, Z. Hu, W. Huang, *Nano Energy* **2015**, 15, 303.
- [89] C. Zhu, T. Liu, F. Qian, W. Chen, S. Chandrasekaran, B. Yao, Y. Song, E. B. Duoss, J. D. Kuntz, C. M. Spadaccini, M. A. Worsley, Y. Li, *Nano Today* **2017**, 15, 107.
- [90] X. Tian, J. Jin, S. Yuan, C. K. Chua, S. B. Tor, K. Zhou, *Adv. Energy Mater.* **2017**, 7, 1700127.
- [91] K. Fu, Y. Yao, J. Dai, L. Hu, *Adv. Mater.* **2017**, 29, 1603486.
- [92] K. Fu, Y. Wang, C. Yan, Y. Yao, Y. Chen, J. Dai, S. Lacey, Y. Wang, J. Wan, T. Li, Z. Wang, Y. Xu, L. Hu, *Adv. Mater.* **2016**, 28, 2587.
- [93] W. Yu, H. Zhou, B. Q. Li, S. Ding, *ACS Appl. Mater. Interfaces* **2017**, 9, 4597.
- [94] K. Sun, T.-S. Wei, B. Y. Ahn, J. Y. Seo, S. J. Dillon, J. A. Lewis, *Adv. Mater.* **2013**, 25, 4539.
- [95] P. Du, X. Hu, C. Yi, H. C. Liu, P. Liu, H.-L. Zhang, X. Gong, *Adv. Funct. Mater.* **2015**, 25, 2420.
- [96] P. Yang, X. Xiao, Y. Li, Y. Ding, P. Qiang, X. Tan, W. Mai, Z. Lin, W. Wu, T. Li, H. Jin, P. Liu, J. Zhou, C. P. Wong, Z. L. Wang, *ACS Nano* **2013**, 7, 2617.
- [97] L. Yuan, X. Xiao, T. Ding, J. Zhong, X. Zhang, Y. Shen, B. Hu, Y. Huang, J. Zhou, Z. L. Wang, *Angew. Chem.* **2012**, 124, 5018.
- [98] Y. Liu, B. Weng, J. M. Razal, Q. Xu, C. Zhao, Y. Hou, S. Seyedin, R. Jalili, G. G. Wallace, J. Chen, *Sci. Rep.* **2015**, 5, 17045.
- [99] G. Wang, H. Wang, X. Lu, Y. Ling, M. Yu, T. Zhai, Y. Tong, Y. Li, *Adv. Mater.* **2014**, 26, 2676.
- [100] X. Wang, B. Liu, Q. Wang, W. Song, X. Hou, D. Chen, Y.-b. Cheng, G. Shen, *Adv. Mater.* **2013**, 25, 1479.
- [101] S. Jung, J. Lee, T. Hyeon, M. Lee, D.-H. Kim, *Adv. Mater.* **2014**, 26, 6329.
- [102] Y. Ai, Z. Lou, S. Chen, D. Chen, Z. M. Wang, K. Jiang, G. Shen, *Nano Energy* **2017**, 35, 121.
- [103] N. A. Kyeremateng, T. Brousse, D. Pech, *Nat. Nanotechnol.* **2016**, 12, 7.
- [104] M. Beidaghi, C. Wang, *Adv. Funct. Mater.* **2012**, 22, 4501.
- [105] W.-W. Liu, Y.-Q. Feng, X.-B. Yan, J.-T. Chen, Q.-J. Xue, *Adv. Funct. Mater.* **2013**, 23, 4111.
- [106] J. Lin, C. Zhang, Z. Yan, Y. Zhu, Z. Peng, R. H. Hauge, D. Natelson, J. M. Tour, *Nano Lett.* **2013**, 13, 72.
- [107] Z.-S. Wu, K. Parvez, A. Winter, H. Vieker, X. Liu, S. Han, A. Turchanin, X. Feng, K. Müllen, *Adv. Mater.* **2014**, 26, 4552.
- [108] B. Song, L. Li, Z. Lin, Z.-K. Wu, K.-s. Moon, C.-P. Wong, *Nano Energy* **2015**, 16, 470.
- [109] J. Yun, Y. Lim, G. N. Jang, D. Kim, S.-J. Lee, H. Park, S. Y. Hong, G. Lee, G. Zi, J. S. Ha, *Nano Energy* **2016**, 19, 401.
- [110] M. Zhu, Y. Huang, Y. Huang, H. Li, Z. Wang, Z. Pei, Q. Xue, H. Geng, C. Zhi, *Adv. Mater.* **2017**, 29, 1605137.
- [111] Z. Liu, S. Liu, R. Dong, S. Yang, H. Lu, A. Narita, X. Feng, K. Müllen, *Small* **2017**, 13, 1603388.
- [112] J. Luo, F. R. Fan, T. Jiang, Z. Wang, W. Tang, C. Zhang, M. Liu, G. Cao, Z. L. Wang, *Nano Res.* **2015**, 8, 3934.
- [113] S. Gong, W. Schwalb, Y. Wang, Y. Chen, Y. Tang, J. Si, B. Shirinzadeh, W. Cheng, *Nat. Commun.* **2014**, 5, 3132.
- [114] B. Y. Lim, J. Yoon, J. Yun, D. Kim, S. Y. Hong, S. J. Lee, G. Zi, J. S. Ha, *ACS Nano* **2014**, 8, 11639.
- [115] D. Kim, D. Kim, H. Lee, Y. R. Jeong, S.-J. Lee, G. Yang, H. Kim, G. Lee, S. Jeon, G. Zi, J. Kim, J. S. Ha, *Adv. Mater.* **2016**, 28, 748.
- [116] D. Qi, Z. Liu, Y. Liu, W. R. Leow, B. Zhu, H. Yang, J. Yu, W. Wang, H. Wang, S. Yin, X. Chen, *Adv. Mater.* **2015**, 27, 5559.